Available online at www.sciencedirect.com
SCIENCE DIRECT®
International Journal of Heat and Mass Transfer 47 (2004) 3057–3071
International Journal of HEAT and MASS TRANSFER
www.elsevier.com/locate/ijhmt

Tube bundle flows with the large Eddy simulation technique in curvilinear coordinates

Y.A. Hassan *, H.R. Barsamian

Department of Nuclear Engineering, Texas A&M University, College Station, TX 77843-3133, USA

Received 4 October 2003; received in revised form 27 February 2004

Abstract

Large Eddy simulation (LES) of a three-dimensional tube bundle at Reynolds number of 21,700, based on the inlet velocity and the tube diameter was performed. The numerical predictions were compared with available data. The calculations are consistent with the experimental data. The 'flapping' effect in the tube wake was captured. This investigation indicates that the large Eddy simulation technique can be utilized as a tool in predicting the unsteady behavior of flow in some industrial applications.

1. Introduction

Flow induced vibration (FIV) results in the motion of a body under alternating direction forces caused by a fluid on an object of interest. The objects that obstruct the flow are known as bluff bodies. In the field of nuclear engineering, bluff bodies are found in heat exchangers where boundary layer separation and vortex shedding are common. The periodic separation of eddies from the cylinders results into unsteady flow field, which produces oscillating forces acting on the cylinders. These oscillatory forces can excite structural vibrations. In heat exchangers, bluff bodies are tube arrays that experience fluid elastic instability (dominant cause of failure in heat exchanger tube bundles) and turbulent buffeting (contributes to long term wear) [1]. Therefore, understanding the pertinent fluid mechanics is important in order to improve the design of such engineering structures.

Current predictions of FIV in heat exchanger tube arrays are not completely reliable and available data are incomplete. There are opportunities for better predictive tools, such as the unsteady semi-analytical model by Granger and Gay [2], the quasi-steady model by Granger and Paidoussis [3], the non-linear analysis method by Rzentkowski and Lever [4], and inverse methods for the measurement of fluid elastic forces by Hadj-Sadok et al. [5]. Experiments can provide measurements of specific phenomena caused by flow-induced vibrations, but detailed full-field data necessary for analysis are often difficult and expensive to obtain, if possible at all. On the other hand, the increasing level of performance of computers and improvements in numerical techniques have made the numerical simulation of turbulent flows in complex geometries an attractive complement to experimental measurements, thereby increasing the demand for new and more accurate numerical methods.

Description of the flow evolution in a tube bundle is significant both theoretically and practically. The available data for the flow in tube bundles can be the theoretical basis for the testing and improvement of numerical methods, turbulence models, and wall models for such geometric configurations. Understanding the flow characteristics can be the practical basis for designing more efficient and durable heat exchangers for power generation [6].

Detailed experimental data in tube bundles for turbulent flows are sparse. Most available data on tube banks (whether rigid or flexible tubes) are concerned with pressure drops, heat transfer, and visualization of overall flow characteristics. Chen and Jendrzejczyk [7]

* Corresponding author. Tel.: +1-979-845-7090; fax: +1-979-845-6443.
E-mail address: y-hassan@tamu.edu (Y.A. Hassan).

0017-9310/$ - see front matter © 2004 Elsevier Ltd. All rights reserved.
doi:10.1016/j.ijheatmasstransfer.2004.02.026

examined the fluctuating forces on a non-staggered tube bundle with a constant pitch-to-diameter ratio at a range of Reynolds numbers. Similar measurements at varying pitch-to-diameter ratios have been performed by Oengoeren and Ziada [8]. Results in these cases are available in the form of power spectral densities of the lift and drag coefficients. More recently, detailed investigations of mean and turbulence data have become available due to the advancement of accurate measuring techniques. Balabani and Yanneskis [9] give an extensive literature review. Halim and Turner [10] have presented experimental data for the mean velocity and turbulence distributions in several rows of a staggered bundle with a pitch to diameter ratio of 1.58 and Reynolds number between 60,000 and 110,000. Simonin and Barcouda [11] have measured the planar velocity components in a square array with a pitch to diameter ratio of 1.47 and Reynolds number of 18,000 using water as the working fluid. In a later paper Simonin and Barcouda [6] have extended their previous work and measured the flow development across the same staggered arrangement up to the sixth row and the results were compared with predictions from a numerical code using the k–ε turbulence model. Balabani et al. [12] have also performed similar calculations and compared to data they have collected of a flow in the subcritical regime with a large pitch-to-diameter ratio. In their experiments they have shown that vortex shedding and jet flapping may occur in the flow.

The high velocity profiles in the passages of the rods or tubes, and the regions in the wake of the tubes that have lower velocities and observe rotational structures can characterize the flow field in a tube bundle. From these descriptions, one can deduce that the flow in a tube bundle extends through many length scales and is anisotropic. The interaction among these many scales deems the accurate simulation of bundle flows unrealistic using the RANS technique with k–ε or Reynolds stress turbulence models. Although several RANS simulations have been performed as a result of the 2nd and 3rd ERCOFTAC-IAHR workshops [13,14], LES simulations of full bundle fields are lacking. For example, Rollet-Miet et al. [15] performed RANS with k–ε turbulence where mean velocity profiles were well predicted, but the shear stress profiles did not compare well. It has been shown that RANS models give poor predictions of the stresses in the tube wakes [16]. Rodi [17] has also demonstrated that the widely used RANS equations based on the standard turbulence models (e.g., k–ε) are incapable of accurately predicting the vortex-shedding behavior.

The aim of this paper is to present a three-dimensional numerical investigation of a turbulent flow paste a tube bundle using the large Eddy simulation in curvilinear coordinates. The comparison of the calculations with the experimental data is presented. The following section gives a brief overview of the large Eddy simulation technique and closure methods.

2. Turbulence prediction

With large Eddy simulation (LES) the large scales of motion of turbulence are directly calculated, while approximating the small ones. The justification for such a treatment is those the larger eddies contain most of the energy, do most of the transporting of conserved properties, and vary most from flow to flow. The smaller eddies are believed to be more universal and play a less important role and should be easier to model [18].

LES uses a filtering operation to separate the large scales that are to be calculated from the small scales that are to be modeled. This concept of variable separation [19] is similar to that of RANS systems, however the physics is completely different. Filtering generates terms that are unresolved. These unresolved scales in the flow should be modeled using subgrid scale models.

Applying the filtering operation to the incompressible equations of continuity and momentum and using the commutation properties, filtered equations are obtained

$$\frac{\partial \bar{u}_i}{\partial x_i} = 0 \tag{1}$$

$$\frac{\partial \bar{u}_i}{\partial t} + \frac{\partial \bar{u}_i \bar{u}_j}{\partial x_j} = -\frac{1}{\rho}\frac{\partial \bar{p}}{\partial x_i} + \nu \frac{\partial^2 \bar{u}_i}{\partial x_j \partial x_j} - \frac{\partial \tau_{ij}}{\partial x_j} \tag{2}$$

where the subgrid scale (SGS) stress tensor τ_{ij} can be expressed as a function of resolved flow variables. Filtering operation and differentiation do not commute when using curvilinear coordinates. However, Ghosal and Moin [20] in their analysis on LES of complex geometry topologies, they showed that "the use of large Eddy simulation introduces an error that is no more than the error introduced by a second-order difference scheme used to discretize the LES equation". The error in the discretization used in the present analysis of structured mesh arrangement would not therefore be greater than the error found employing the mesh arrangement in Cartesian Coordinates. It is also carefully resolved the flow field close the surfaces with rather compact concentrated mesh to reduce the discretization errors.

The most widely used SGS model is of the Eddy viscosity type and was proposed by Smagorinsky [21]. In the Smagorinsky model, proportionality between the anisotropic part of the SGS stresses and the large-scale strain rate tensor is assumed

$$\tau_{ij} - \frac{1}{3}\delta_{ij}\tau_{kk} = -2\nu_T \overline{S}_{ij} \tag{3}$$

where ν_T is the SGS Eddy viscosity and is generally assumed to be a scalar quantity, and $\overline{S}_{ij}$ is the large-scale

strain rate tensor. The following definition applies for the SGS Eddy viscosity

$$v_T = (C_S \Delta)^2 |\overline{S}| \tag{4}$$

where the local strain rate is defined by

$$|\overline{S}| = (2\overline{S}_{ij}\overline{S}_{ij})^{1/2} \tag{5}$$

$$\overline{S}_{ij} = \frac{1}{2}\left(\frac{\partial \bar{u}_i}{\partial x_j} + \frac{\partial \bar{u}_j}{\partial x_i}\right) \tag{6}$$

and C_S is the model parameter ranging from about 0.065 to 0.25, and Δ is the length scale used in the definition of the filter.

The dynamic subgrid scale (DSGS) model has shown to predict SGS stresses better than the Smagorinsky Eddy viscosity model [22–25]. The dynamically local coefficient C_S is calculated from the simulated resolved scales by applying a test filter which is typically two times coarser than the one used to separate the SGS from the grid scales (GS). The dynamic subgrid scale model used in this investigation has been described in details in Barsamian [26], and Barsamian and Hassan [27]. Time integration scheme was applied so that the Courant number is below one, because otherwise spatially resolvable high-frequent fluctuations are filtered out. The computer program GUSTCC is a finite volume computer program uses a staggered grid formulation to discretize the governing equations. The control volumes are non-orthogonal curvilinear coordinates. Although these cells are irregular in shape and size, they are structured. The solution is second order in space and time. It uses central differencing scheme for spatial discretization and the Crank–Nicolson scheme for temporal discretization. Mittal and Moin [28] have shown that a second-order central difference solution of flow past a cylinder produces better velocity power spectra, when compared to experiments than the higher-order upwind schemes. The numerical diffusion must be much smaller than the diffusion introduced by the SGS model. Breuer [30] also stressed the important aspect of low numerical diffusion in the case for turbulent flow past a circular cylinder. His study confirmed the second order central difference scheme turned out to be well suited for LES. Therefore, in this study, the convective terms of the conservation equations are approximated by second-order central difference. In order to perform some sensitivity studies of the GUSTCC computer program, parameter variations were studied. To assess the effect of the SGS model, we performed simulations with and without the SGS closure model. The simulation without the SGS model did not converge. From this we may conclude that for this Reynolds number with the given grid resolution, the SGS model contribution is significant to the flow and therefore cannot be ignored. Also, it shows that numerical diffusion is minimal [26]. Another test was performed to show if any unacceptable numerical damping was present. In the simulations without a SGS model, the time step was halved twice and applied to the simulation without a SGS model to see if numerical diffusion would cause the flow to converge. No such convergence was seen. Another sensitivity study was performed to ascertain the influence of the grid refinement on the predictions. No appreciable difference in the predictions by halving the node size was obtained.

3. Tube bundle simulation in three dimensions and boundary conditions

The flow in tube bundles is of great interest to the power generation industry, not only for the study of performance of heat exchangers. Safety studies require predictions of vibrations caused by fluid-structure interaction or large temperature fluctuations that eventually lead to thermal stripping. The flow within the bundles experiences complex unsteady behavior, making it an attractive case to be studied using large Eddy simulation technique. Knowledge gained from the previous LES calculations [27,30] has been used in the simulation of a three-dimensional flow in a staggered tube bundle arrangement at a Reynolds number of 21700 based on the freestream velocity and tube diameter. A three-dimensional simulation for LES is required in this type of geometry. Because two-dimensional and three-dimensional turbulence behave differently e.g., three-dimensional treatment is necessary even when the mean flow stays rather two-dimensional. At high Reynolds number situation as in this bundle geometry, the cylinder wake structure is strongly three-dimensional. Therefore, the LES technique is applied in a three dimensional calculation of the staggered tube bundle. Results are compared to the data obtained via laser Doppler velocimetry (LDV) measurements [6,11].

The experimental setup of Simonin and Barcouda [11] consists of a staggered bundle arrangement of seven tube rows in a rectangular channel. Using a steady uniform approach flow, the Reynolds number was measured to be 18000. The spacing between the tube centers (pitch) was 45 mm with tube diameters of 21.7 mm. The height of the channel was 100 mm with the tubes fixed at both ends. The corresponding pitch-to-diameter ratio is 2.07. Using the LDV method, two-dimensional measurements of the mean velocity and stresses were performed. Details of measuring techniques, setup, and error can be found in several articles [6,11].

A schematic of the tube bundle is given in Fig. 1. This geometry is later used in the LES calculations. The general properties of the flow in such a bundle include regions of flow reversal behind the tubes and high

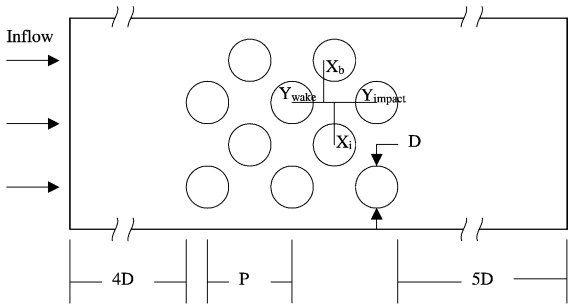

Fig. 1. Schematic of tube bundle.

velocity flow in the passages between the tubes. One of the noted characteristics in the experiments has been the different flow structure as the fluid progressed into the bundle. Barsamian and Hassan [29] observed similar characteristics in a different two-dimensional bundle simulation at a high Reynolds number in a non-staggered arrangement where two pitch lengths were needed for the flow to become fully developed in the bundle. A notable phenomenon observed by Simonin and Barcouda [6] was the large recirculation zone behind the first tube. This recirculation zone decreased in size in subsequent tubes of the bundle. Their measurements also show that a relatively flat mean velocity profile is present in the gaps, and the wakes of the tubes contain the highest turbulence level of the flow.

Our objective is to simulate the bundle flow using the LES technique. Therefore, we have used the Simonin and Barcouda [6] experiment geometry to compare with the calculations. This is one of the first attempts of performing a full three-dimensional bundle simulation using LES in curvilinear coordinates for this type of geometry. One other LES calculation previously performed [15] uses a periodic subsection of the bundle. The integral length scale of a bundle simulation is on the order of the tube diameter, therefore a domain smaller than the pitch length is unreasonable. This is a significant deficiency in their simulation. Also, the periodic boundaries may cause inconsistencies near the entrance and exit regions. In this study a bundle with 5 rows and inlet boundary condition is simulated.

The sketch shown in Fig. 1 illustrates the complete flow simulation area used in this investigation. The streamwise, normal and spanwise directions are, respectively, x, y and z. The dimensions in units of diameter, D, are $4D$ for the inlet development region, 5 rows of tubes and a subsequent $5D$ after the tube bundle. This approach provides buffer regions to uncouple the upstream area from the distortions of the outlet. A spanwise length of $5D$ was used. The sketch delineates the fact that the geometry for the bundle is not symmetric. Wall boundaries were used in all directions except for the inlet and outlet of the flow. Detailed descriptions of the wall and inlet boundary conditions have been presented in details in Barsamian [26], and Barsamian and Hassan [27]. In LES, it is necessary to initialize inlet boundary conditions with some form of perturbation to provide an initial turbulent condition. That is, the turbulent intensity should be specified at each point of the inflow plane. Since the inlet conditions could have a substantial effect on the field downstream, it is important that these perturbations be both spatially and temporally correlated. The inlet boundary condition of the inflow fluctuations was generated for each inlet grid using a zero-mean Gaussian random distribution function. In addition, an entry length section was also applied to the flow geometry whereby at least two integral length scale distances were used for the initial random correlation effects to diminish. The combination of these two approaches of specifying random velocity fluctuations that satisfy some given constraints and then allow the flow to develop helps to trigger better estimation of the fluctuations. The exit boundary conditions are extended downstream to a distance of 5D from the last row of cylinders to exclude the influence of outlet boundary. A new wall model based on modification of Werner and Wengle wall model [32] is used. Due to the complex geometry of the bundle walls, curvilinear coordinates are utilized to refine the wall modeling.

The discretization of the flow domain uses $236\times122\times37$ control volumes in a body fitted coordinate system, of which 982,800 were active control volumes while the remaining were used to apply the boundary conditions. The control volumes are refined in the tube bundle region. Fig. 2 gives the nodalization of the entire domain, while Fig. 3 shows a subsection of the tube bundle. There are no highly skewed grids and grid distribution has been concentrated near the tube walls to provide a better description of the boundary layer. A substantial amount of grid points are also accommodated in the region between the cylinders to resolve the wake region.

An overview of scales within the domain under the simulated experimental conditions is given in Table 1. The parameters are within suggested limits for a LES calculation [22]. The simulations are performed at a Reynolds number of 21700 based on the inlet velocity and tube diameter. This corresponds to a Reynolds number of 42000 based on the gap velocity and tube diameter. A uniform approach flow of 1.0 m/s is used on which maximum turbulence intensity of 5% is added. A time step value of 5×10^{-5} s was used which yielded a courant number of 0.25 (below 1). A total of 1024 time steps are utilized for simulation analysis after the flow reaches a quasi-steady state mode. The following sections will describe the unsteady three-dimensional results obtained using the LES computer program [26,31].

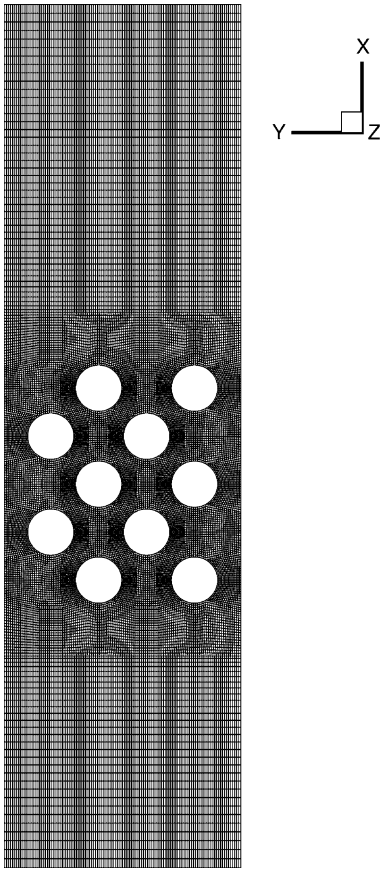

Fig. 2. Nodalization of entire simulation tube bundle.

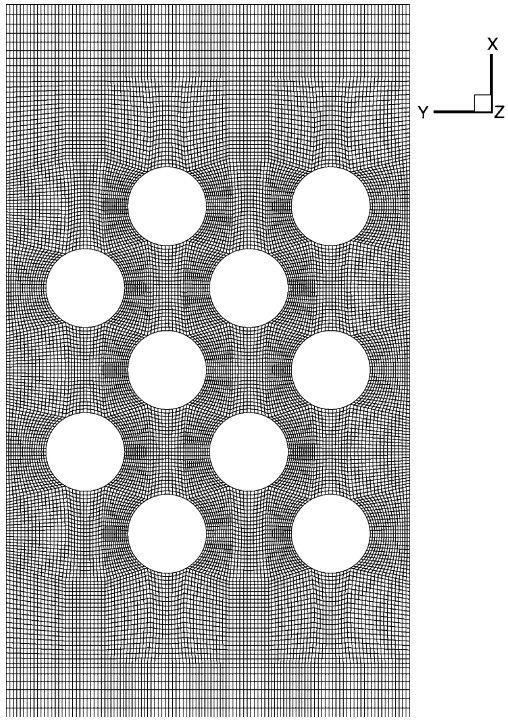

Fig. 3. Nodalization of bundle section.

Table 1
Tube bundle simulation details

Inlet velocity	1.0 m/s
Kolomogorov length	$\sim 1.2\times10^{-5}$ m
Taylor microscale	$\sim 5.7\times10^{-4}$ m
Grid size	$\sim 2\times10^{-4}$ m
Minimum time resolution	$\sim 1\times10^{-4}$ s
Actual time step	$\sim 5\times10^{-5}$ s
Courant number CFL	0.25

4. Results and discussion

Visualization results are presented in sets of several time steps for a half of a shedding cycle with 0.0025 s between each frame. Unless otherwise stated, the results only show the section containing the tube bundle (inlet and outlet developing regions are not presented). Visualization will include the following variables: velocity vectors, velocity magnitude, pressure contours, vorticity, and swirling strength. It should be noted that in the previous work referenced, visualization have been performed on the mean quantities, while here, the transient phenomena is discussed in addition to the mean quantities.

Figs. 4 and 5 delineate the total velocity vectors and pressure contours of the selected region at two different time steps at the bundle midplane. The arrows are proportional to the velocity magnitude. Highest-pressure gradients occur at the top of the bundle between the tubes and the wall. The difference between the top and bottom pressure contours is due to the non-symmetric nature of the bundle geometry. The pressure contours also indicate a relatively constant pressure in the passages between the tubes. The pressure contours in the wake and impact zones of the tubes fluctuate in a manner consistent with the flapping motion discussed below. The velocity vectors indicate high flow rates in the passages and recirculation zones in the wake of the tubes. Movement of the transverse motion in the recirculation zones is apparent when comparing the different time steps. Fig. 6 delineates the non-dimensional pressure contours in the same region for the last frame.

Contours of the normalized velocity magnitude are shown in Figs. 7 and 8. The shedding occurs in the wake of the tubes. The mass flow distribution on the sides of a central tube is not negligible and not similar because of the shedding effect generated by the non-symmetric nature of the geometry and the higher Reynolds number of the flow. The highest velocity values are near the top tubes of the channel indicated by the contour values and

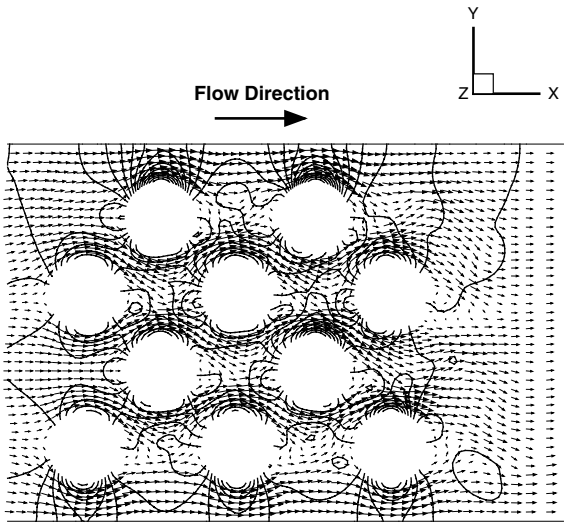

Fig. 4. Velocity vectors and pressure contours for tube bundle for frame 1.

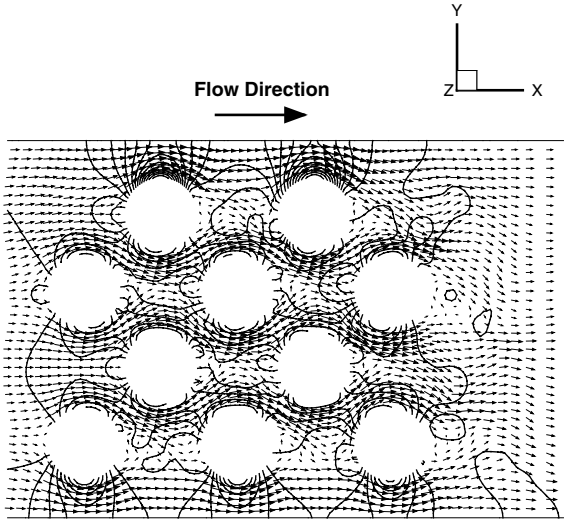

Fig. 5. Velocity vectors and pressure contours for tube bundle for frame 2.

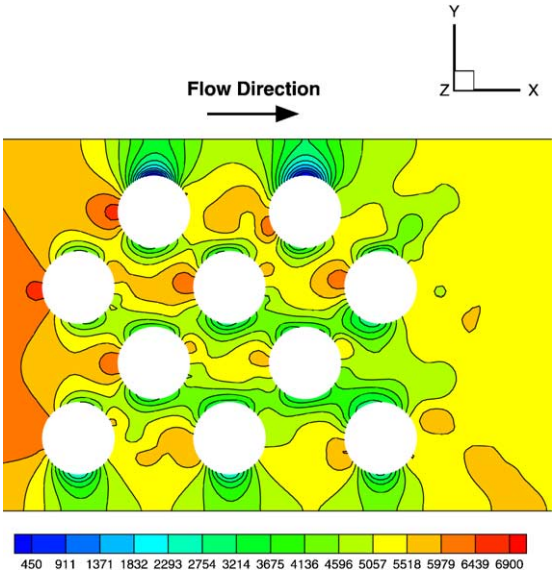

Fig. 6. Dimensionless pressure contours for tube bundle for frame 2.

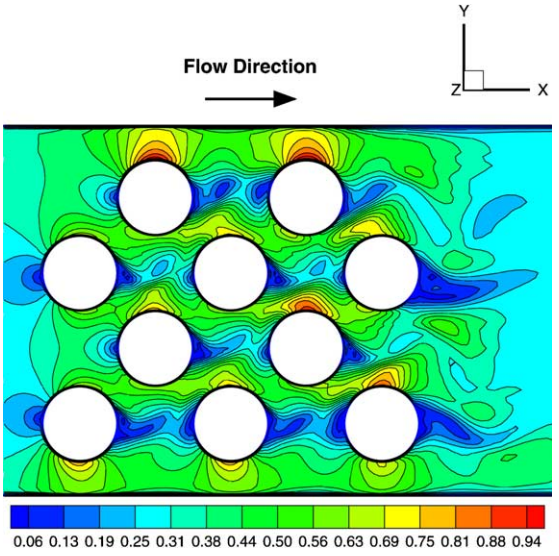

Fig. 7. Normalized velocity magnitude at midplane for tube bundle for frame 1.

the lowest velocity values are in the wake of the tubes. The wakes of the exit row tubes are larger. This is due to the absence of inhibiting flow by the next row of tubes as the situation was in the bundle. The mean velocity gradient is negligible in the narrow passages shown by the constant contour profile.

Enhanced visualization of the shedding process can be seen through the vorticity magnitude for the same temporal profile as shown in Figs. 9 and 10. Three definitive characteristics can be explained. First, the largest rotational structures in the flow occur in the tube wakes and are generated due to viscous forces. Second, there is a clear shedding of the vortices behind the tubes. Third, the rotating structures that separate because of the shedding are carried from the low velocity region into the high velocity region in a manner comparable to the shedding frequency from either side of a given tube. These in turn affect the flow in the open channel region between the tubes. As we will see, these do not drasti-

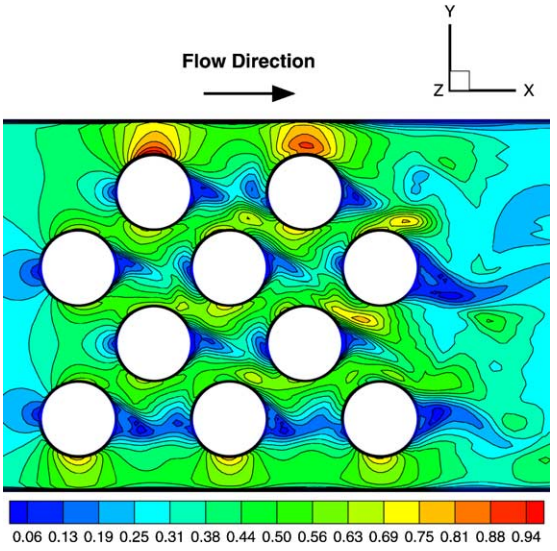

Fig. 8. Normalized velocity magnitude at midplane for tube bundle for frame 2.

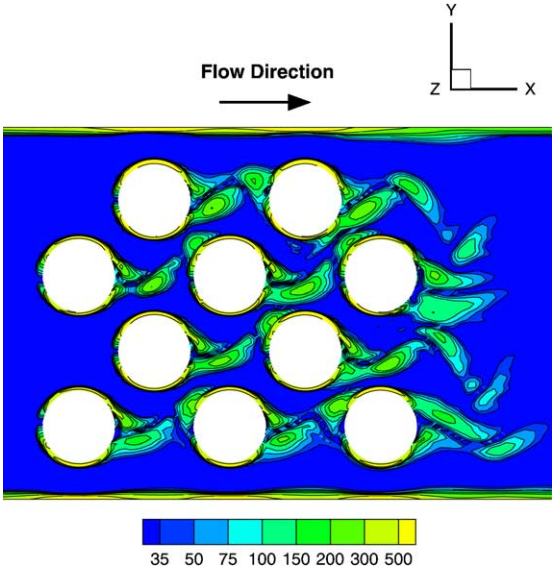

Fig. 9. Vorticity magnitude at midplane for tube bundle for frame 1.

cally affect the mean profile of the flow, but have some effect on the stresses when compared to the experimental data. The occurrence possibility of this phenomenon has been suggested by Balabani et al. [12]. They have termed it as a 'flapping' phenomenon. This is clearly observed in the LES calculations. Rollet-Miet et al. [15] have also discussed this phenomenon in terms of the 'wall echo effect'. These are initiated by the detached low velocity regions from the cylinder wake and get transported to-

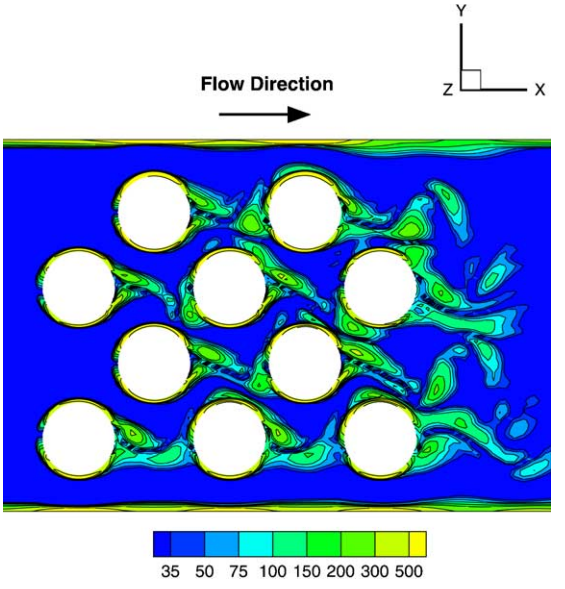

Fig. 10. Vorticity magnitude at midplane for tube bundle for frame 2.

wards the impact tube. The fluctuations of these regions could be significant. The 'wall echo effect' explains the transformation of the wall normal fluctuations into the lateral fluctuations. These in turn could affect the turbulence intensity of the spanwise flow, which is assumed negligible in most flows. In Fig. 11 the three-dimensional vorticity magnitude is shown for contour level of 85 Hz.

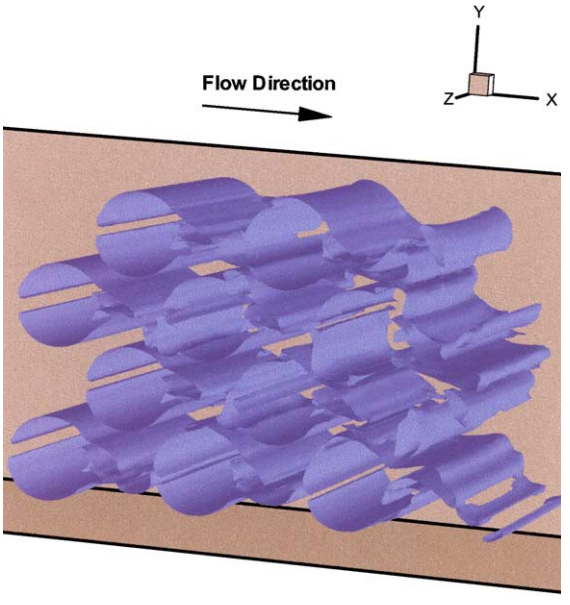

Fig. 11. Three-dimensional vorticity magnitudes plot at contour level of 85 Hz for tube bundle.

Except for near the wall regions, two-dimensionality of the flow is delineated.

To visualize the effects of three-dimensionality in the flow and its transient behavior, the x-component of vorticity is shown in Figs. 12 and 13. Solid line contours indicate positive vorticity values, while the dashed lines have negative vorticity. The figures show a cut in the y–z plane across the tube centers in the fourth row. Two pairs of counter-rotating vortices are seen in the region between the tubes. These are very strong near the tube ends. They disappear at the bundle midplane indicating a relative absence of large-scale three-dimensional effects at the midplane. However, as stated above, the 'wall echo effect' could enhance turbulence quantities in the spanwise direction. Balabani et al. [12] have also suggested that two-dimensionality may be assumed, but they reached such a conclusion using mean velocity profiles.

In order to compare with experimental data of Simonin and Barcouda [6,11], results of the LES calculation are extracted at locations shown in Fig. 1. All values are normalized using the free stream velocity of 1.0 m/s. The Reynolds number of the LES calculation was 21700 and was slightly higher than the original experimental value of 18000. Also, as noted earlier, the non-symmetric nature of the tube bundle has shown vortex shedding that causes 'flapping'. Accuracy of the experimental measurements near the tube wall is questionable with the closest measured distance on the order of 2 mm.

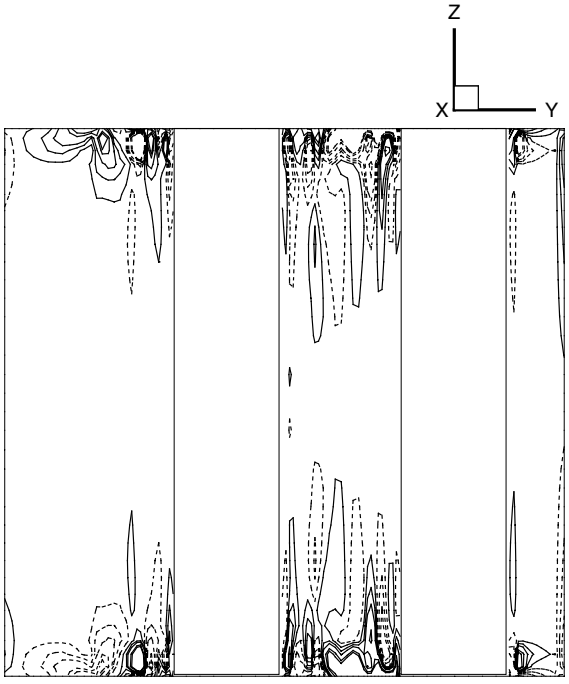

Fig. 12. X-vorticity for tube bundle for frame 1.

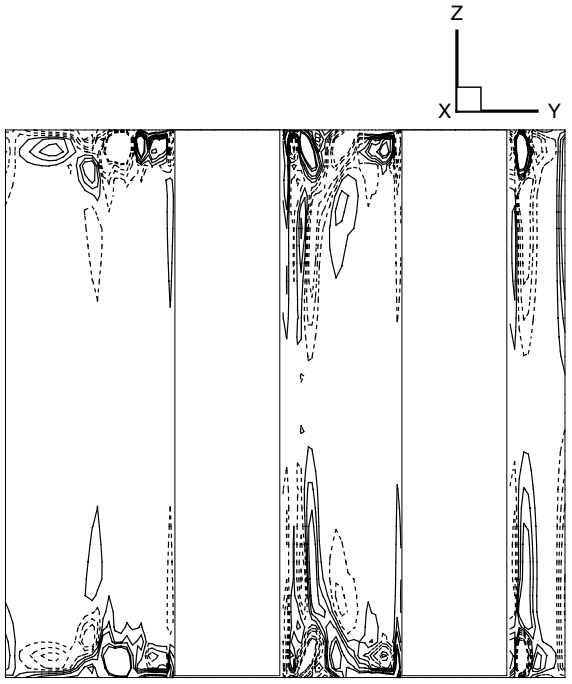

Fig. 13. X-vorticity for tube bundle for frame 2.

In this study a movie is generated from the computational experiment. It shows the vortex evolution. It indicates that the vortex is shed and convected downstream. While convected, the vortex is deformed and squeezed. The vortex path changes from one instant to the other. It switches between the up and below paths.

The axial positions at X_i and X_b in Figs. 14(a)–(e) and 15(a)–(e), respectively, represent the typical mean and stress profiles in the bundle. It is indicated that minimum streamwise velocity values decrease as the position shifts from X_i to X_b. The highest velocity is near the tube in the passage. The V-shaped profile in the wake region is visible as well. The mean velocity in the transverse direction is nearly negligible except for near the center of the gap (where it is highest) indicating the shedding of the flow and as seen earlier, vorticity is highest within this region. There is a good agreement between the experimental data and LES calculations for the mean streamwise and transverse velocities.

The shear stresses at these axial locations are considered next. These are shown in Figs. 14(c)–(e) and 15(c)–(e). The $\langle uu \rangle$ normal stress values increase with increasing distance from the tube and are nearly constant in the main stream. They slightly increase near the end of the recirculation zones before decreasing again. The LES calculation captures the correct magnitude; however, some variations in profile are present. There are two 'humps', one that occurs in the passage and another in the recirculation region. The 'hump' in the

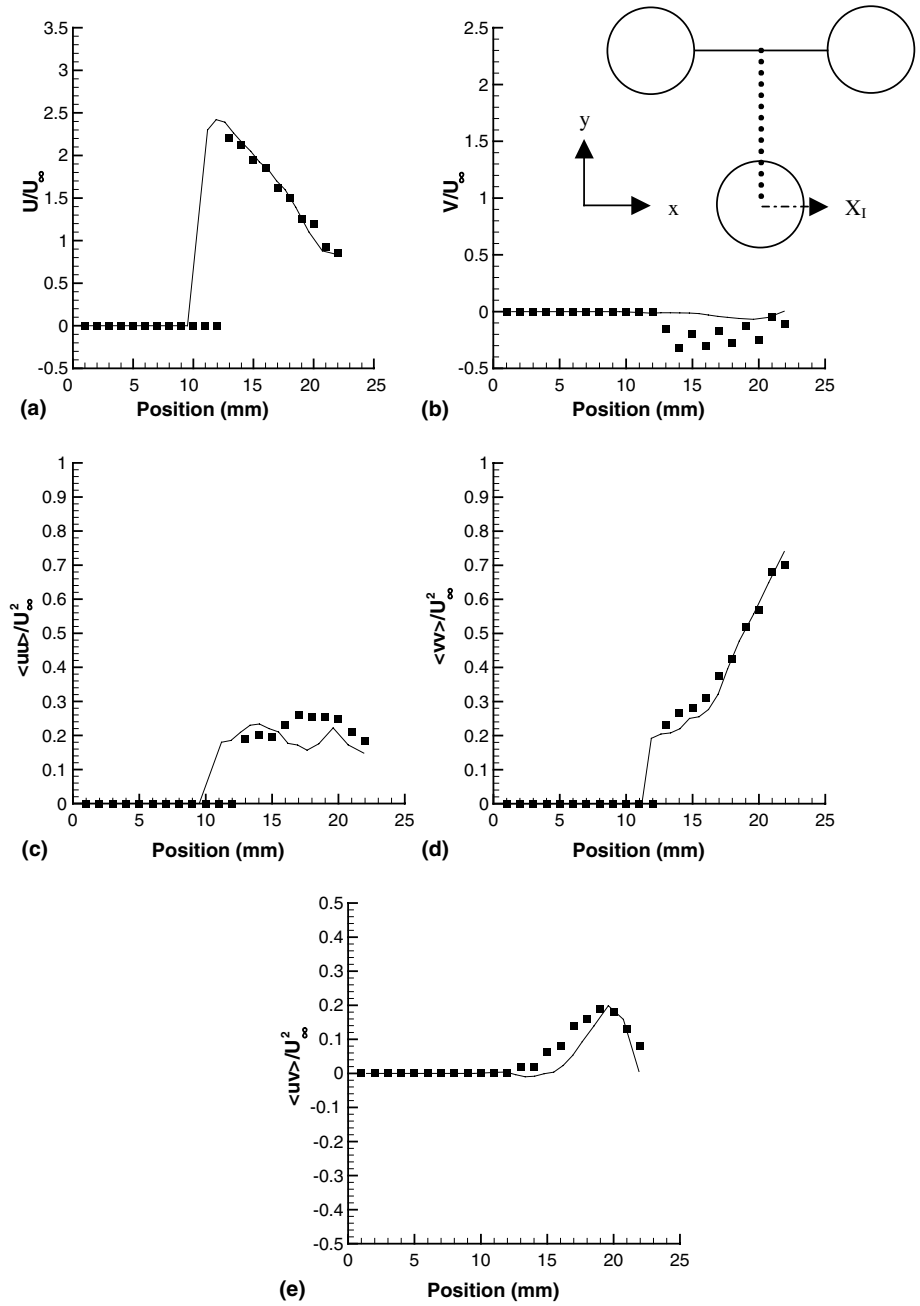

Fig. 14. Comparison between LES calculations and experiment at X_I.

passage corresponds to the increased turbulence due to the 'flapping' of the flow where packets of fluid from the recirculation region are released into the passages. The 'hump' in the recirculation region corresponds to the vortex formation section due to shear. The $\langle vv \rangle$ normal stress exhibits a different behavior. These values are highest in the recirculation region indicating intense lateral mixing and decrease rapidly due to dissipation and negative production. The cross terms of Reynolds stress prediction values are also in good agreement with the experimental data. The highest Reynolds stress values occur in the recirculation regions. The shear stress values have been normalized by the square of the upstream velocity, U_∞.

In a similar fashion, the positions indicated by Y_{wake} and Y_{impact} in Fig. 1 are delineated in Figs. 16(a)–(e) and

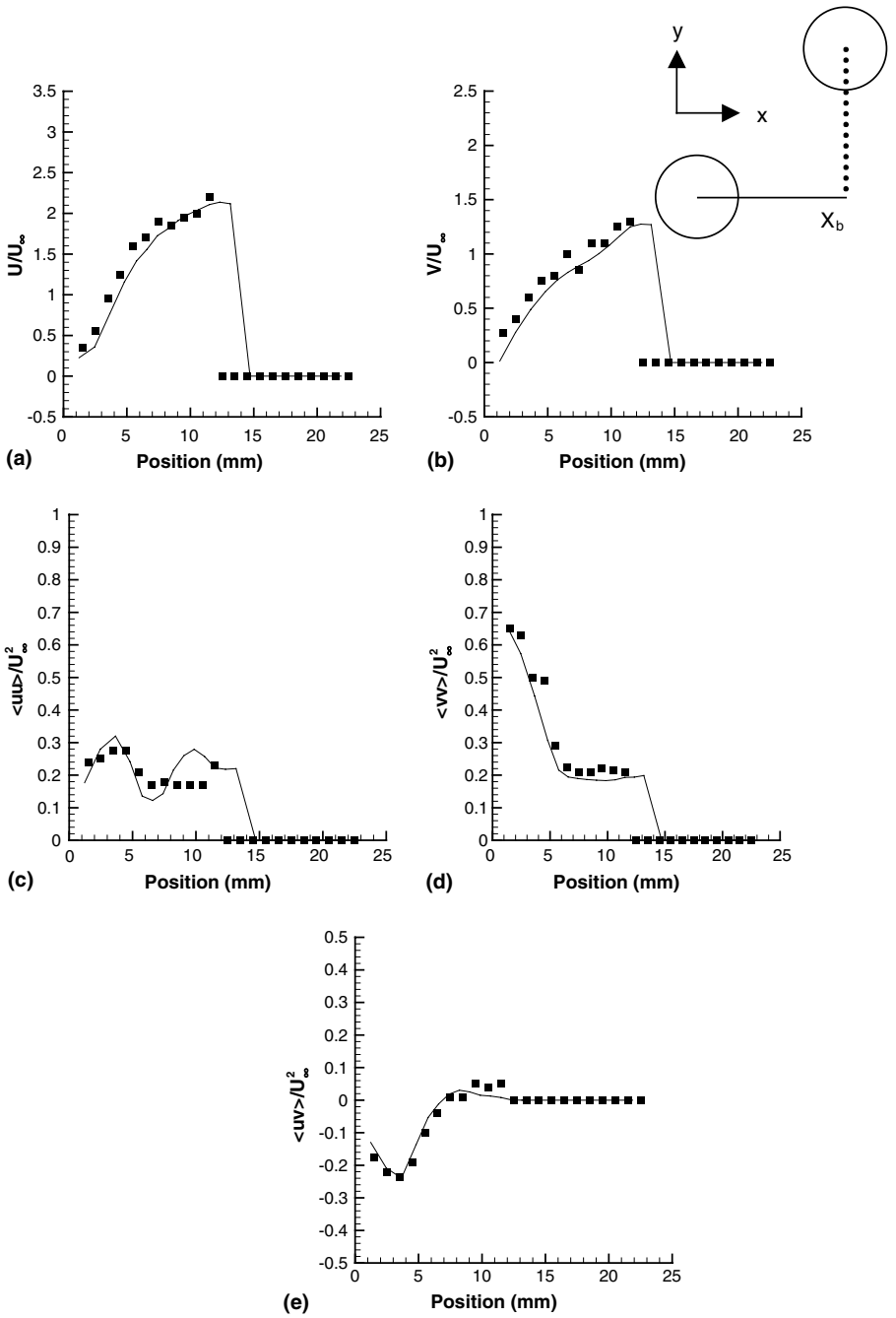

Fig. 15. Comparison between LES calculations and experiment at X_b.

17(a)–(e), respectively. The mean velocities are in a good agreement. The experimental data does not capture the recirculation region that occurs in the wake of a tube. The LES calculations clearly depict the effect by the negative value of the streamwise velocity near the Y_{wake} tube. However, we should be caution, in comparing the LES results for these regions to the experimental data. The Reynolds stresses capture the magnitude of the respective coefficients compared with the experimental data.

Contours of the total viscosity for the bundle region are plotted in Fig. 18 for a given frame. As the figure delineates, the mean viscosity value in the bulk of the flow is relatively constant. Viscosity is highest in the

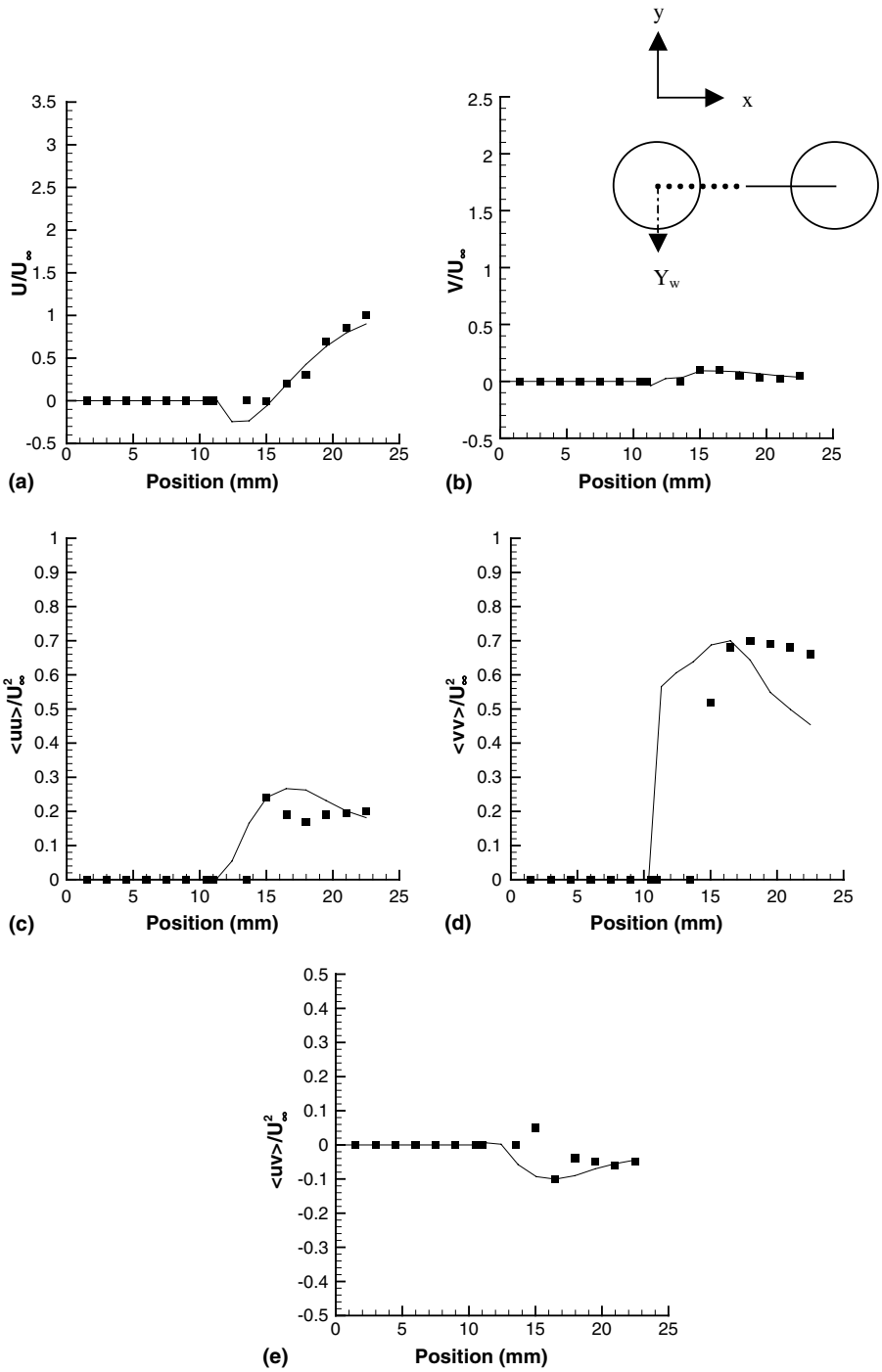

Fig. 16. Comparison between LES calculations and experiment at Y_{wake}.

wake of the tubes, especially within the vortex structures. The unfiltered and filtered values of the dynamic subgrid model coefficient at a location in the wake of the tube are shown in Fig. 19. There are large variations for the unfiltered value of the model coefficient. Although the filtered value has some variation, it is close to a mean value of 0.01. It should be noted that this value corresponds to 0.1 of the Smagorinsky model

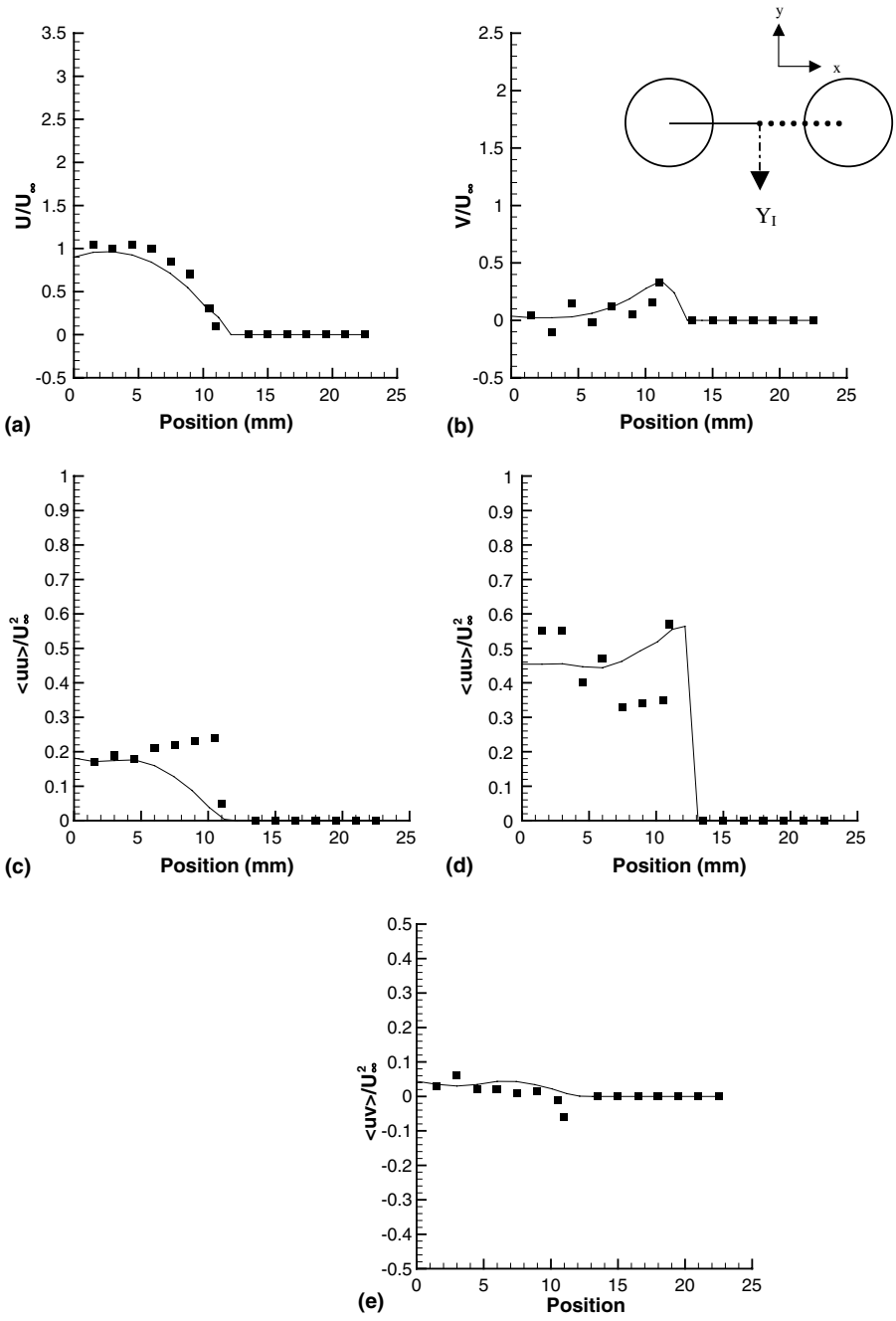

Fig. 17. Comparison between LES calculations and experiment at Y_{impact}.

coefficient. This is a typical value used as the coefficient for the Smagorinsky model. The benefit of using dynamic model is also that it does not require preliminary tuning for the specific nature of the flow as in Smagorinsky scale. Therefore, it is believed to be safer for an over cost of computation less than 5%.

Power density distribution (PSD) and correlation functions are considered for acceptable decay behavior of the turbulent quantities. The PSD plot of the gap velocities is given in Fig. 20(a), while the PSD of the lift force and drag force coefficients is shown in Fig. 20(b). The gap velocity PSD shows an acceptable decay pattern

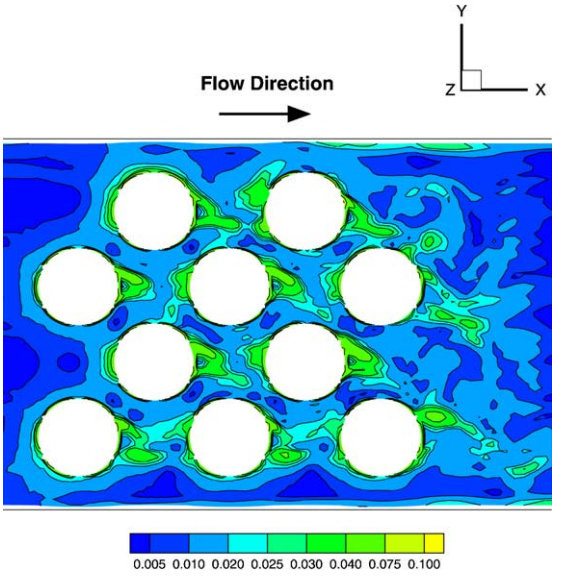

Fig. 18. Viscosity (m^2/s) contours in tube bundle for frame 2.

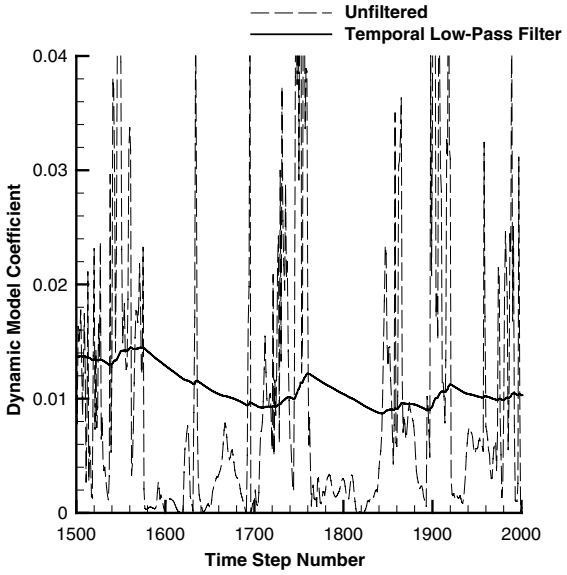

Fig. 19. Dynamic model coefficient as a function of time step.

where the inertial subrange region covers about a decade in frequency. There are no distinct Strouhal peaks as in the case of the single tube simulation [26]. The lift and drag coefficient PDS plots are shown with the bound spectrum curve. The bound spectrum represents an upper bound PSD in developed flows [28]. The coefficient PSD values are within bound spectrum limits and agree with bound spectra of Oengoeren and Ziada [8].

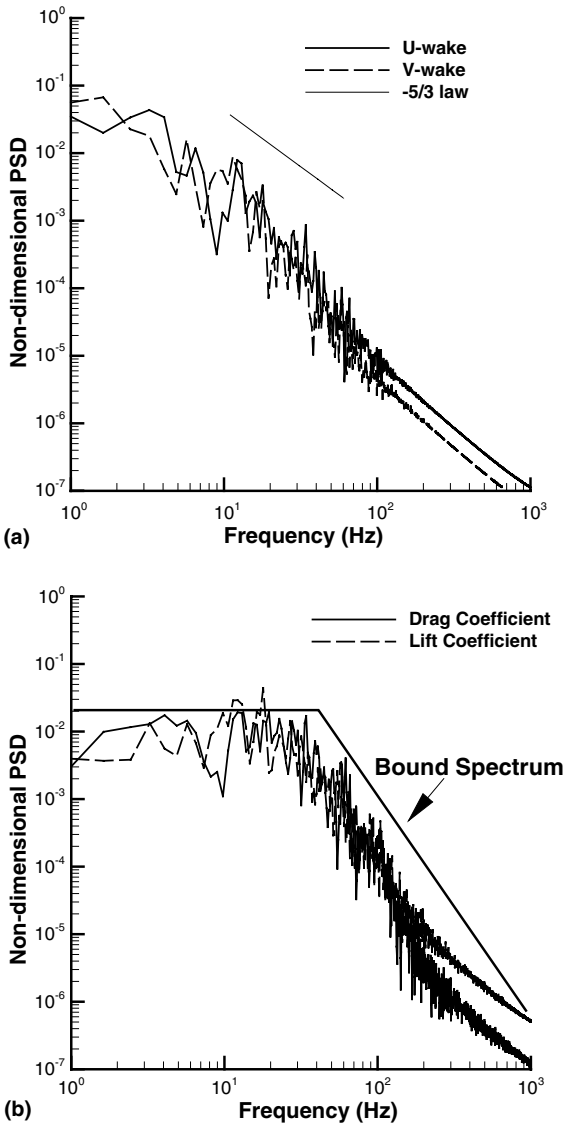

Fig. 20. Non-dimensional (a) velocity and (b) force PSD as a function of frequency.

Auto-correlation functions are given in Fig. 21(a) and (b) for the streamwise and transverse velocities at several locations. The correlation in the streamwise direction (Fig. 21(a)) in the passage and wake are similar, with a correlation time of 0.0125 s. This corresponds to a length scale of 0.01125 m, which is close to the integral length scale of the bundle (0.0217 m). The lag time in the passage for the transverse velocity (Fig. 21(b)) is much shorter than in the wake. This indicates that transverse turbulence intensities in the wake are relatively high.

The cross-correlation data in Fig. 21(c) and (d) are those of in the tube wake. The streamwise velocity

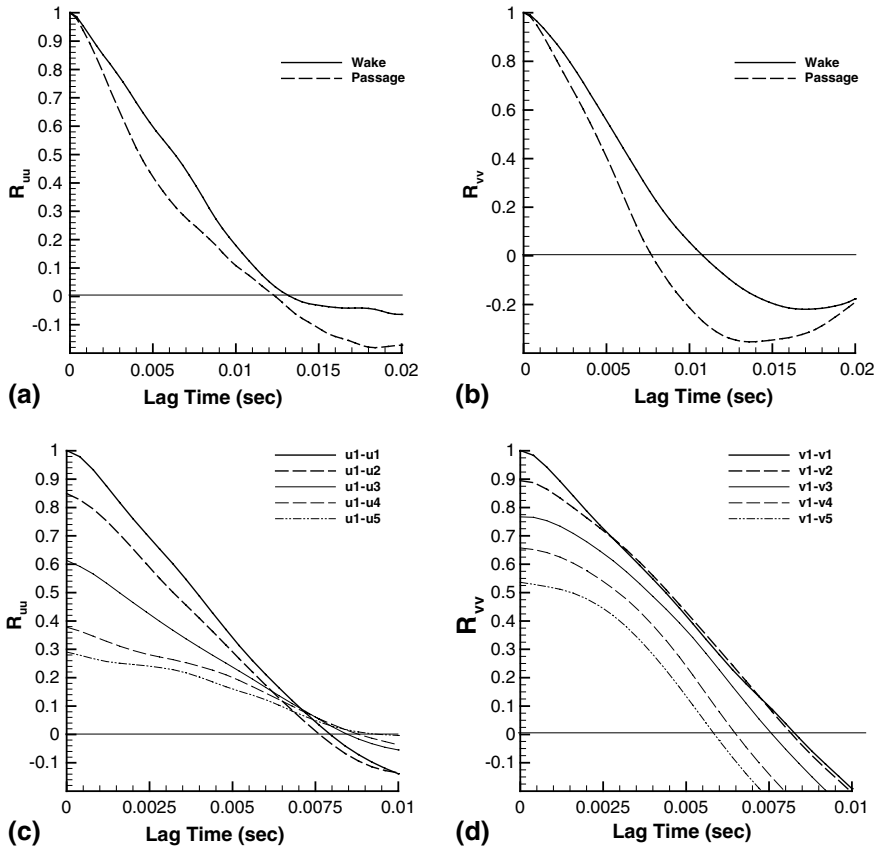

Fig. 21. Auto-correlation and cross-correlation as a function of lag time.

correlation is at five locations in the positive x-direction, while the transverse velocity correlation is at five locations in the positive y-direction. The distance between each point was constant. The correlation curves indicate decay in association as the distance between two points is increased. The association in the transverse direction decreases faster as the points get farther apart.

5. Conclusion

The flow behavior in a tube bundle using the LES technique is simulated. Three-dimensional curvilinear coordinates are used to obtain better refinement of the bundle complex geometry. Fine nodalization is implemented close to the wall boundaries. Visualization results capture experimentally observed phenomena. Calculations comparison with experiments is in a good agreement. Reynolds stresses are in a reasonable agreement with the experimental data. Understanding the flow structure within flow bundles could assist in alleviating problems associated with flow-induced vibration and noise.

References

[1] R.D. Blevins, Flow Induced Vibration, second ed., Van Nostrand Reinhold, New York, 1990.
[2] S. Granger, N. Gay, An unsteady semi-analytical model for cross-flow induced vibration of tube bundles: Comparison with experiments, in: P.W. Bearman (Ed.), Flow-Induced Vibration, A.A. Balkema, Rotterdam, Netherlands, 1995, pp. 327–338.
[3] S. Granger, M.P. Paidoussis, An improvement to the quasi-steady model with application to cross-flow induced vibration of tube arrays, in: P.W. Bearman (Ed.), Flow-Induced Vibration, A.A. Balkema, Rotterdam, Netherlands, 1995, pp. 339–350.
[4] G. Rzentkowski, J.H. Lever, An effect of turbulence on fluid elastic instability in tube bundles: A nonlinear analysis, in: P.W. Bearman (Ed.), Flow-Induced Vibration, A.A. Balkema, Rotterdam, Netherlands, 1995, pp. 351–362.
[5] C. Hadj-Sadok, E. de Langre, S. Granger, Inverse methods for the measurement of fluid elastic forces in tube bundles, in: P.W. Bearman (Ed.), Flow-Induced Vibration, A.A. Balkema, Rotterdam, Netherlands, 1995, pp. 363–371.
[6] O. Simonin, M. Barcouda, Measurements and prediction of turbulent flow entering a staggered tube bundle, in: 4th

International Symposium on Applications of Laser Anemometry to Fluid Mechanics, Lisbon, Portugal, paper 5.23, 1988.
[7] S. Chen, J. Jendrzejczyk, Fluid excitation forces acting on a tube array, ASME J. Fluids Eng. 109 (1987) 415–423.
[8] A. Oengoeren, S. Ziada, Unsteady fluid forces acting on a square tube bundle in air cross-flow, in: Symposium on Flow Induced Vibration and Noise, Montreal, Canada, vol. 230, 1992, pp. 55–74.
[9] S. Balabani, M. Yanneskis, Flow and heat transfer characteristics of tube bundles in crossflow, Department of Mechanical Engineering Report EM/93/05, King's College, London, 1993.
[10] M.S. Halim, J.T. Turner, Measurements of cross flow development in a staggered tube bundle, in: 3rd International Symposium on Applications of Laser Anemometry to Fluid Mechanics, Lisbon, Portugal, paper 21.7, 1986.
[11] O. Simonin, M. Barcouda, Measurements of fully developed turbulent flow across tube bundle, in: 3rd International Symposium on Applications of Laser Anemometry to Fluid Mechanics, Lisbon, Portugal, paper 21.5, 1986.
[12] S. Balabani, G. Bergeles, D. Burry, M. Yanneskis, Velocity characteristics of the crossflow over tube bundles, in: 7th International Symposium on Applications of Laser Anemometry to Fluid Mechanics, Lisbon, Portugal, vol. 2, 1994, pp. 39.3.1–39.3.8.
[13] ERCOFTAC-IAHR workshop, 2nd ERCOFTAC-IAHR Workshop on Refined Flow Modelling, Lisbon, Portugal, 1993.
[14] ERCOFTAC-IAHR workshop, 3rd ERCOFTAC-IAHR Workshop on Refined Flow Modelling, UMIST (The University of Science and Technology in Manchester), Manchester, United Kingdom, 1994.
[15] P. Rollet-Miet, D. Laurence, J. Ferziger, LES and RANS of turbulent flow in tube bundles, Int. J. Heat Fluid Flow 20 (1999) 241–254.
[16] J.K. Watterson, W.N. Dawes, A.M. Savill, A.J. White, Predicting turbulent flow in a staggered tube bundle, Int. J. Heat Fluid Flow 20 (1999) 581–591.
[17] W. Rodi, Comparison of LES and RANS calculation of the flow around bluff bodies, J. Wind Eng. Indus. Aerodyne. 69–71 (1997) 55–75.
[18] J.H. Ferziger, Large Eddy simulation: An introduction and perspective, in: O. Metais, J. Ferziger (Eds.), New Tools in Turbulence Modelling, Springer, Berlin, 1996, pp. 29–47.
[19] A. Leonard, Energy cascade in large-Eddy simulations of turbulent fluid flows, Adv. Geophys. A 18 (1974) 237–248.
[20] S. Ghosal, P. Moin, The basic equations for large Eddy simulation of turbulent flows in complex geometry, J. Comput. Phys. 118 (1995) 24–37.
[21] J. Smagorinsky, General circulation experiments with primitive equations, Monthly Weather Rev. 91 (1963) 216–241.
[22] U. Piomelli, Large Eddy simulation of turbulent flows, Theoretical and Applied Mathematics, TAM Report No. 767 (UILU-ENG-94-6023), University of Illinois at Urbana-Champaign, Urbana, IL, 1994.
[23] E. Balaras, Finite-difference computations of high Reynolds number flows using the dynamic subgrid-scale model, Theor. Comput. Fluid Dyn. 7 (1995) 207–218.
[24] S. Ghosal, T. Lund, P. Moin, A dynamic localization model for large-Eddy simulation of turbulent flows, Annual Research Briefs, Center for Turbulence Research, Stanford, California, 1993.
[25] Y. Zang, R.L. Street, J.R. Koseff, A dynamic mixed subgrid-scale model and its application to turbulent recirculating flows, Phys. Fluids A 5 (12) (1993) 3186–3196.
[26] H.R. Barsamian, New near-wall models with dynamic subgrid scale closure for large Eddy simulation in curvilinear coordinates for complex geometries, PhD dissertation, Texas A&M University, College Station, TX, 2000.
[27] H.R. Barsamian, Y.A. Hassan, New wall modeling for complex flows using the large Eddy simulation technique in curvilinear coordinates, Int. J. Heat Mass Transfer 44 (21) (2001) 4009–4026.
[28] R. Mittal, P. Moin, Suitability of upwind-biased finite difference schemes for large Eddy simulation of turbulent flows, AIAA J. 35 (1997) 1415–1417.
[29] H.R. Barsamian, Y.A. Hassan, Large Eddy simulation of turbulent cross flow in tube bundles, Nucl. Eng. Design 172 (1997) 103–122.
[30] M. Breuer, Large Eddy simulation of the subcritical flow past a circular cylinder: Numerical and modeling aspects, Int. J. Numer. Methods Fluids 28 (1998) 1281–1302.
[31] M.J. Budden, P.J. Dionne, N. Vaidya, A.D. Leonard, GUSTCC: A large Eddy simulation computer code for steam generator applications: Theory manual, CFDRC Report 4038/3, CFD Research Corporation, Huntsville, AL, 1994.
[32] H. Werner, H. Wengle, Large Eddy simulation of turbulent flow over and around a cube in a plate channel, in: 8th Symposium on Turbulent Shear Flows, Munich, Germany, 1991.